

Transverse Polarization of Top Quark Pairs at the Tevatron and the Large Hadron Collider*

Werner Bernreuther, Arnd Brandenburg, and Peter Uwer

*Institut für Theoretische Physik, Physikzentrum
Rheinisch-Westfälische Technische Hochschule Aachen
52056 Aachen, Germany*

Abstract

We investigate the prospects to observe effects of transverse polarization of top quarks in $pp, p\bar{p} \rightarrow t\bar{t}X$. QCD absorptive parts generate a polarization of top quarks and antiquarks transverse to the production plane in the partonic processes $q\bar{q} \rightarrow t\bar{t}$ and $gg \rightarrow t\bar{t}$, which reaches values of a few percent. These perturbative QCD effects are decreased at the hadronic level. A measurement through momentum correlations among the t and \bar{t} decay products will be difficult both at an upgraded Tevatron and at the LHC.

*supported by BMBF Contract 056AC92PE

1 Introduction

The existence of the top quark has recently been firmly established [1]. Combining the measurements of the CDF and D0 experiments, the mass of the top quark is $m_t = 179 \pm 12$ GeV. Detailed studies of the properties of top quarks will be a main objective of experiments at present and future colliders. With an expected luminosity of $\mathcal{L} \sim 2 \times 10^{32} \text{cm}^{-2} \text{s}^{-1}$, the upgraded Tevatron collider will produce several thousand top quark pairs per year, and the Large Hadron Collider (LHC) is even expected to yield several million top quark pairs per year. These event rates will allow for precision experiments with top quarks.

A special feature of physics with top quarks is due to their heaviness: Because of its large mass, the top quark has decayed on average before it can form hadronic bound states. In particular, the polarization of the top quark is not diluted by hadronization, and observables involving the spin of the top quark may therefore be calculated reliably within perturbation theory. Moreover, the t and \bar{t} analyze their spins through their parity-violating weak decays $t \rightarrow Wb$. Effects connected with the spin of the top quark can then be used to test the standard model (SM) or to search for new physics, as has been realized and investigated by many authors (see, e.g., [2]–[19], and references quoted therein).

In this paper we will concentrate on studying a possible polarization of the t and \bar{t} transverse to the production plane in proton-proton and proton-antiproton collisions. This transverse polarization is odd under simultaneous reflection of spins and momenta (i.e., odd under the “naive” time reversal operation T_N). To leading order, it is directly proportional to the absorptive part of the scattering amplitude if the true time reversal operation is a good symmetry of the theory. In particular, it probes QCD at the one-loop level without having to contend with the usual large tree level “background”.

The main production mechanism for $t\bar{t}$ -pairs in hadronic collisions are the parton subprocesses $q\bar{q} \rightarrow t\bar{t}$ and $gg \rightarrow t\bar{t}$. QCD absorptive parts giving rise to a transverse polarization of the top quark and antiquark have been calculated for these parton processes first by Dharmaratna and Goldstein [6], [7]. Their result for $gg \rightarrow t\bar{t}$ was used by Kane,

Ladinsky and Yuan to estimate the size of transverse polarization to be expected at LHC energies and beyond [10]. We reanalyze this subject for two reasons: First, because the process $q\bar{q} \rightarrow t\bar{t}$ is dominant at the Tevatron and the corresponding transverse polarization phenomena at the hadronic level have not been studied before. Second, we would like to present realistic numbers for directly measurable quantities sensitive to the transversely polarized top quarks. These quantities are T_N -odd momentum correlations of the decay products of the t and \bar{t} . The outline of our paper is as follows: In the next section, we will give analytic results for the transverse polarization of t and \bar{t} in $q\bar{q} \rightarrow t\bar{t}$ and $gg \rightarrow t\bar{t}$ to order α_s , point out a slight difference to existing results [6], and discuss the effects on parton level. In section 3, we will proceed by constructing suitable observables to trace these effects in top pair production at hadron colliders. The corresponding T_N -odd momentum correlations will require a measurement of momenta of final state particles only. The statistical significance of these correlations will be discussed for the Tevatron and the LHC.

2 Transverse Polarization in $q\bar{q} \rightarrow t\bar{t}$ and $gg \rightarrow t\bar{t}$

In this section we will define transverse polarization of top quarks and antiquarks in terms of the production density matrices for the partonic subprocesses $q\bar{q} \rightarrow t\bar{t}$ and $gg \rightarrow t\bar{t}$, which are the dominant production mechanisms for top quark pair production at the Tevatron and the LHC, respectively. We will give analytic results for the transverse polarization of t and \bar{t} induced by QCD absorptive parts at the one-loop level.

We first turn to the reaction $q(p_1) + \bar{q}(p_2) \rightarrow t(k_1) + \bar{t}(k_2)$, where the momenta refer to the $q\bar{q}$ center of mass system, $\mathbf{p}_1 + \mathbf{p}_2 = 0$. In order to discuss polarization phenomena for t and \bar{t} , we define the (unnormalized) production density matrix

$$R_{\alpha_1\alpha_2,\beta_1\beta_2}^q(\mathbf{p}, \mathbf{k}) = \frac{1}{4} \frac{1}{N_C^2} \sum_{\text{colors}, q\bar{q} \text{ spins}} \langle t(k_1, \alpha_1)\bar{t}(k_2, \beta_1) | \mathcal{T} | q(p_1), \bar{q}(p_2) \rangle^* \langle t(k_1, \alpha_2)\bar{t}(k_2, \beta_2) | \mathcal{T} | q(p_1), \bar{q}(p_2) \rangle. \quad (1)$$

Here, α, β are spin indices, N_C denotes the number of colors, $\mathbf{p} = \mathbf{p}_1$, $\mathbf{k} = \mathbf{k}_1$ and the

sum runs over the colors of all quarks and over the spins of q and \bar{q} . The factor $1/4 \cdot 1/N_C^2$ takes care of the averaging over spins and colors in the initial state. The matrix structure of R^q in the spin spaces of t and \bar{t} is

$$R^q = A^q \mathbb{1} \otimes \mathbb{1} + \mathbf{B}_t^q \cdot \boldsymbol{\sigma} \otimes \mathbb{1} + \mathbf{B}_{\bar{t}}^q \cdot \mathbb{1} \otimes \boldsymbol{\sigma} + C_{ij}^q \sigma^i \otimes \sigma^j, \quad (2)$$

where σ^i are the Pauli matrices and the first (second) factor in the tensor products refers to the t (\bar{t}) spin space. For a detailed discussion of R^q and its symmetry properties, see [15]. For the purpose of this paper, it is sufficient to note that absorptive parts in the parton scattering amplitude due to CP - and P - invariant interactions yield the following contribution to the production density matrix:

$$R_{\text{abs}}^q = b_3^q(\hat{s}, z) \hat{\mathbf{n}} \cdot \{ \boldsymbol{\sigma} \otimes \mathbb{1} + \mathbb{1} \otimes \boldsymbol{\sigma} \}, \quad (3)$$

where $\hat{s} = (p_1 + p_2)^2$, $z = \hat{\mathbf{p}} \cdot \hat{\mathbf{k}}$ is the cosine of the scattering angle in the partonic center of mass frame, $\hat{\mathbf{n}} = (\mathbf{p} \times \mathbf{k})/|\mathbf{p} \times \mathbf{k}|$ is the normal to the scattering plane, and $b_3^q(\hat{s}, z)$ is a structure function in the notation of [15]. The production density matrix $R^g(\mathbf{p}, \mathbf{k})$ for the subprocess $g(p_1) + g(p_2) \rightarrow t(k_1) + \bar{t}(k_2)$ is defined, in the gg center of mass frame, in complete analogy to Eq. (1) with $1/N_C^2 \rightarrow 1/(N_C^2 - 1)^2$. Due to Bose symmetry of the gluon-gluon initial state we have for the corresponding structure function:

$$b_3^g(\hat{s}, z) = -b_3^g(\hat{s}, -z). \quad (4)$$

The transverse polarization P_\perp of the top quark is equal to the transverse polarization of the top antiquark in a CP invariant theory and given for the respective subprocesses by

$$P_\perp^i = \langle \hat{\mathbf{n}} \cdot \boldsymbol{\sigma} \otimes \mathbb{1} \rangle_i \equiv \frac{\text{tr}(R^i \hat{\mathbf{n}} \cdot \boldsymbol{\sigma} \otimes \mathbb{1})}{\text{tr} R^i} = \frac{b_3^i(\hat{s}, z)}{A^i(\hat{s}, z)} \quad (i = q, g). \quad (5)$$

The functions $A^i(\hat{s}, z)$ are related to the differential cross section of the respective partonic subprocess:

$$A^i(\hat{s}, z) = \frac{8\pi \hat{s}}{\beta} \frac{d\hat{\sigma}^i}{dz}, \quad (6)$$

where $\beta = \sqrt{1 - 4m_t^2/\hat{s}}$ is the velocity of the top quark in the partonic c.m. system. In leading order of the QCD coupling, they have the well-known form [20] (which we give here for completeness):

$$A^q(\hat{s}, z) = \pi^2 \alpha_s^2 \frac{N_C^2 - 1}{N_C^2} [2 - \beta^2(1 - z^2)], \quad (7)$$

$$A^g(\hat{s}, z) = \pi^2 \alpha_s^2 \frac{2[-2 + N_C^2(1 + \beta^2 z^2)]}{N_C(N_C^2 - 1)(1 - \beta^2 z^2)^2} [1 + 2\beta^2(1 - z^2)(1 - \beta^2) - \beta^4 z^4]. \quad (8)$$

In A^q we neglected the masses of the quarks in the initial state.

Nonvanishing $b_3^i(\hat{s}, z)$ are generated by QCD absorptive parts at the one-loop level through interference with the tree graphs. Other standard model contributions, like from absorptive parts of diagrams with Higgs or Z bosons, are tiny and therefore we neglect them. Before presenting our results, we would like to comment briefly on the details of the calculation. We performed two independent calculations of the functions $b_3^i(\hat{s}, z)$, one using conventional covariant gauge Feynman rules, the other using the background field method [21]. The background field method greatly facilitates the calculation of b_3^g , and, because of gauge invariance, gives the same final result as the conventional approach. In Fig. 1 (2) we show the one-loop Feynman diagrams which give a nonzero contribution to b_3^q (b_3^g) in the conventional approach. Although the final results are ultraviolet and infrared finite, one has to use a regularization scheme in intermediate steps to handle divergent integrals. We used dimensional regularization. Moreover, we eliminated the usual box integral in four dimensions in favor of a linear combination of a six-dimensional box integral and four triangle integrals [22]. This method shifts all infrared divergencies into the triangle integrals, and the cancellation of the infrared divergencies becomes completely explicit.

For $q\bar{q} \rightarrow t\bar{t}$ we get:

$$b_3^q = \frac{\pi \alpha_s^3 (N_C^2 - 1)}{2N_C^2} \frac{m_t}{\sqrt{\hat{s}}} \sqrt{1 - z^2} (N_C g_1 + \frac{g_2}{N_C}),$$

with

$$g_1 = -\frac{\pi}{\beta^2} \left[(1 - \beta^2) \ln \left(\frac{1 + \beta}{1 - \beta} \right) - 2\beta \right] - \frac{\pi z}{2\beta^3} \left[3(1 - \beta^2) \ln \left(\frac{1 + \beta}{1 - \beta} \right) - 6\beta + 4\beta^3 \right],$$

$$g_2 = \frac{4\pi}{\beta^2} \left[(1 - \beta^2) \ln \left(\frac{1 + \beta}{1 - \beta} \right) - 2\beta \right] + \pi\beta z. \quad (9)$$

This result agrees with the one given in [7].

For $gg \rightarrow t\bar{t}$, the result is more complex:

$$b_3^g = \frac{2\pi\alpha_s^3}{N_C^2 - 1} m_t \beta \sqrt{\hat{s}} \sqrt{1 - z^2} (N_C^2 f_1 + N_C f_2 + f_3 + \frac{f_4}{N_C^2}),$$

with

$$\begin{aligned} f_1 &= \frac{1 - \beta^2}{2(1 - z\beta)^2} \text{Im}D_0^{D=6}(z) - \frac{1 - \beta^2}{2(1 + z\beta)^2} \text{Im}D_0^{D=6}(-z) \\ &\quad - \frac{z(1 - \beta^2)(1 - 8\beta^2 - 3z^2 - \beta^2 z^2 + 3\beta^2 z^4)}{4\beta(1 - z^2\beta^2)^2} \text{Im}C_0 \\ &\quad - \frac{z(1 - 4\beta^2 - 3z^2 + 2\beta^2 z^2)}{2\beta\hat{s}(1 - z^2\beta^2)} \text{Im}B_0, \\ f_2 &= \sum_i \theta(\sqrt{\hat{s}}/2 - m_i) \frac{z\beta(1 - \beta_i^2)}{2(1 - z^2\beta^2)} \left[\frac{\pi}{\hat{s}} \ln \left(\frac{1 + \beta_i}{1 - \beta_i} \right) - \frac{2\pi\beta_i}{\hat{s}} \right], \\ f_3 &= \frac{\beta}{4(1 - z^2\beta^2)} \left[-(3\beta^2 + z^2 - 6\beta z + 2\beta^2 z^2) \text{Im}D_0^{D=6}(z) \right. \\ &\quad \left. + (3\beta^2 + z^2 + 6\beta z + 2\beta^2 z^2) \text{Im}D_0^{D=6}(-z) - \frac{2z(1 - \beta^2)}{\beta} \text{Im}C_0 \right. \\ &\quad \left. - \frac{2z(2 + 5\beta^2 - \beta^2 z^2)}{\hat{s}\beta} \text{Im}B_0 \right], \\ f_4 &= \frac{\beta}{2(1 - z^2\beta^2)} \left[-\frac{(3\beta^2 + z^2 - 6\beta z + 2\beta^2 z^2)}{1 - z\beta} \text{Im}D_0^{D=6}(z) \right. \\ &\quad \left. + \frac{(3\beta^2 + z^2 + 6\beta z + 2\beta^2 z^2)}{1 + z\beta} \text{Im}D_0^{D=6}(-z) \right. \\ &\quad \left. - \frac{2z(1 - \beta^2)(1 - 3\beta^2)}{\beta(1 - z^2\beta^2)} \text{Im}C_0 - \frac{4z}{\hat{s}\beta} \text{Im}B_0 \right]. \end{aligned} \quad (10)$$

Here, $D_0^{D=6}$ stands for a box integral in six dimensions, B_0 and C_0 are usual two-point and three-point scalar one-loop integrals, respectively. The explicit formulae for the imaginary parts are:

$$\begin{aligned} \text{Im}D_0^{D=6}(z) &= -\frac{\pi}{\hat{s}\beta^2} \left\{ \frac{1 + \beta}{1 + z} \ln \left(1 - \frac{\beta(1 + z)}{1 + \beta} \right) + \frac{1 - \beta}{1 - z} \ln \left(1 + \frac{\beta(1 - z)}{1 - \beta} \right) \right\}, \\ \text{Im}C_0 &= \frac{-\pi}{\hat{s}\beta} \ln \left(\frac{1 + \beta}{1 - \beta} \right), \\ \text{Im}B_0 &= \pi. \end{aligned} \quad (11)$$

The sum in f_2 defined in Eq. (10) runs over all quark flavors and $\beta_i = \sqrt{1 - 4m_i^2/\hat{s}}$, where m_i denotes the mass of a quark with flavor i . Numerically, only the top quark gives a significant contribution to f_2 . Our result for b_3^g disagrees slightly with the one given in formula (1) of [6] (and formula (19) of [7]). We find that $f_1 - f_1^{DG} = -\frac{\pi z \beta}{48 \hat{s}(1 - z^2 \beta^2)}$, where f_1 is the leading color coefficient of Eq. (10) and f_1^{DG} is the corresponding term in [6], [7]. We agree[†] with the authors of [6], [7] that this difference is due to the omission of one of the two ghost triangle diagrams (cf. Fig. 2) in the result of [6], [7].

In Figs. 3 and 4 we plot the transverse polarization P_\perp^q and P_\perp^g , respectively, as a function of the partonic c.m. energy $\sqrt{\hat{s}}$ and z , the cosine of the scattering angle. We do not include the running of α_s here, but fix it at the value $\alpha_s = 0.1$. For the top quark mass we used $m_t = 180$ GeV. For quark–antiquark annihilation, the transverse polarization of the top quark reaches values of about 2.5% around $\sqrt{\hat{s}} \simeq 720$ GeV and scattering angle of $\simeq 73$ degrees and then decreases quite rapidly with energy. In the case of gluon–gluon fusion, P_\perp^g nicely exhibits the antisymmetry with respect to z following from Bose symmetry and P_\perp^g reaches peak values of about 1.5% around $\sqrt{\hat{s}} \simeq 1050$ GeV and at $\simeq \pm 63$ degrees. We will discuss in the next section whether these effects are observable at colliders.

3 T_N -odd momentum correlations for semileptonic $t\bar{t}$ decays

The transverse polarization of t and \bar{t} discussed in the previous section must be traced in the final states into which t and \bar{t} decay. We concentrate here on decay modes where one of the top quarks decays semileptonically and the other one decays hadronically, i.e. on samples of $t\bar{t}$ pairs with:

$$\begin{aligned} t &\rightarrow \ell^+ + \nu_\ell + b, \\ \bar{t} &\rightarrow W^- + \bar{b} \rightarrow q + \bar{q}' + \bar{b}, \end{aligned} \tag{12}$$

[†]G. Goldstein, private communication

and the corresponding charge conjugated decay channels. These samples are especially suited for constructing observables which are sensitive to transversely polarized top quarks: The charged lepton of the semileptonic decay serves as an efficient analyzer of the top quark spin [8], while in the same event the purely hadronic decay allows one to reconstruct the momentum of the other top quark. Specifically, for $p\bar{p} \rightarrow t\bar{t}X$ with subsequent semileptonic $t\bar{t}$ decay we define the observable

$$\mathcal{O}_1 = \hat{\mathbf{p}}_p \cdot (\hat{\mathbf{q}}_{\ell^+} \times \hat{\mathbf{k}}_{\bar{t}}) \quad (13)$$

for the decay modes (12), and

$$\bar{\mathcal{O}}_1 = \hat{\mathbf{p}}_p \cdot (\hat{\mathbf{q}}_{\ell^-} \times \hat{\mathbf{k}}_t) \quad (14)$$

for the charge conjugated decays. Here, $\hat{\mathbf{p}}_p$ is the proton's direction (which we take to be the positive z direction of the laboratory coordinate system), \mathbf{q}_{ℓ^\pm} is the momentum of the positively (negatively) charged lepton, hats denote unit vectors and all momenta are defined in the hadronic c.m. system. A T_N -odd correlation may now be defined through the sum:

$$\mathcal{S}_1 \equiv \langle \mathcal{O}_1 \rangle_{\bar{t}\ell^+} + \langle \bar{\mathcal{O}}_1 \rangle_{t\ell^-}, \quad (15)$$

where $(\bar{t}\ell^+)$ refers to sample (12) (reconstructed flight directions of \bar{t} and of the positively charged lepton from t decay) and $(t\ell^-)$ refers to the charge conjugated sample. Gluon-gluon fusion does not contribute to either of the two terms on the r.h.s. of (15) due to Bose symmetry, but this does not lead to a significant decrease of the signal in the case of $p\bar{p}$ collisions around a c.m. energy $\sqrt{s} = 1.8$ TeV, because in this energy regime the contribution of the partonic subprocess $q\bar{q} \rightarrow t\bar{t}$ strongly dominates. Since the unpolarized $p\bar{p}$ initial state is a CP eigenstate, the correlation (15) can only become nonzero through CP conserving interactions. Furthermore, $\langle \mathcal{O}_1 \rangle_{\bar{t}\ell^+} = \langle \bar{\mathcal{O}}_1 \rangle_{t\ell^-}$, if CP is conserved. Taking the difference instead of the sum in (15) gives a T_N -odd, CP -odd correlation, which might be also an interesting quantity to look at in $t\bar{t}$ production.

For pp collisions, each of the two expectation values in (15) vanishes for the following reason: The contribution from $gg \rightarrow t\bar{t}$ again vanishes due to Bose symmetry, and also the

subprocess $q\bar{q} \rightarrow t\bar{t}$ now gives zero, because the contributions of the two partonic initial states ($q \in p(\mathbf{p}_p), \bar{q} \in p(-\mathbf{p}_p)$) and ($\bar{q} \in p(\mathbf{p}_p), q \in p(-\mathbf{p}_p)$) cancel. Suitable observables in the case of pp collisions are given by:

$$\mathcal{O}_2 = -\mathcal{O}_1 \text{sign}(\hat{\mathbf{p}}_p \cdot \hat{\mathbf{k}}_{\bar{t}}), \quad (16)$$

for sample (12), and

$$\bar{\mathcal{O}}_2 = \bar{\mathcal{O}}_1 \text{sign}(\hat{\mathbf{p}}_p \cdot \hat{\mathbf{k}}_t) \quad (17)$$

for the charge conjugated sample. The sum of the expectation values,

$$\mathcal{S}_2 \equiv \langle \mathcal{O}_2 \rangle_{\bar{t}\ell^+} + \langle \bar{\mathcal{O}}_2 \rangle_{t\ell^-}, \quad (18)$$

is a good T_N -odd correlation to trace the transverse polarizations of t and \bar{t} produced in pp collisions. Note that $\langle \mathcal{O}_2 \rangle_{\bar{t}\ell^+} \neq \langle \bar{\mathcal{O}}_2 \rangle_{t\ell^-}$ even in the absence of CP violation. This is because the pp initial state has no definite CP parity. In fact, since quarks on average carry more of the proton's energy than antiquarks, QCD absorptive parts in the $q\bar{q}$ annihilation subprocess lead to a nonvanishing value for the difference

$$\Delta_2 \equiv \langle \mathcal{O}_2 \rangle_{\bar{t}\ell^+} - \langle \bar{\mathcal{O}}_2 \rangle_{t\ell^-} \quad (19)$$

in pp collisions.

We evaluated the correlation \mathcal{S}_1 for $p\bar{p}$ c.m. energies \sqrt{s} between 1.5 TeV and 5.0 TeV and the two correlations \mathcal{S}_2 and Δ_2 for pp collisions with \sqrt{s} between 7 TeV and 20 TeV, using the narrow width approximation for t and \bar{t} . (For a recent discussion of effects of non-factorizable diagrams see [23].) We found only a weak dependence of our results on the choice of the parton distribution functions; in the results below we used the parametrization [24]. For the scale entering the parton distributions we set $Q^2 = 4m_t^2$. Since the results of sect. 2 constitute the lowest order contributions to our correlations, we use leading order distribution functions and a fixed value of $\alpha_s = 0.1$.

Fig. 5 shows the correlation \mathcal{S}_1 for proton-antiproton scattering as a function of the collider c.m. energy. The correlation decreases with rising energy; at $\sqrt{s} = 1.8$ TeV it

has the value $\mathcal{S}_1 \simeq 0.43\%$. The rapidity distribution

$$\langle \mathcal{O}_1 \delta(r_{\bar{t}} - r'_{\bar{t}}) \rangle_{\bar{t}\ell^+} \quad (20)$$

where

$$r_{\bar{t}} = \frac{1}{2} \ln \frac{E_{\bar{t}} + \hat{\mathbf{p}}_p \cdot \mathbf{k}_{\bar{t}}}{E_{\bar{t}} - \hat{\mathbf{p}}_p \cdot \mathbf{k}_{\bar{t}}} \quad (21)$$

is shown in Fig. 6 for $\sqrt{s} = 1.8$ TeV. Note that the distribution is not symmetric in $r_{\bar{t}}$. The corresponding rapidity distribution for the sample with reconstructed top momenta,

$$\langle \bar{\mathcal{O}}_1 \delta(r_t - r'_t) \rangle_{t\ell^-} \quad (22)$$

is equal to the one of Fig. 6 after a reflection at the line $r_{\bar{t}} = 0$.

Fig. 7 shows both \mathcal{S}_2 and Δ_2 for proton–proton collisions with c.m. energies covering 7–20 TeV. The correlation \mathcal{S}_2 reaches a value of $\sim 0.03\%$ at $\sqrt{s} = 14$ TeV. Fig. 8 shows the rapidity distributions (20) and (22) for pp collisions at $\sqrt{s} = 14$ TeV. As discussed above, they are *not* related by a symmetry.

The statistical sensitivity of our observables may be estimated from their root-mean-square fluctuations: For $\sqrt{s} = 1.8$ TeV we find $\Delta\mathcal{O}_1 = \sqrt{\langle \mathcal{O}_1^2 \rangle_{\bar{t}\ell^+} - \langle \mathcal{O}_1 \rangle_{\bar{t}\ell^+}^2} \approx \Delta\bar{\mathcal{O}}_1 \simeq 0.36$. This yields an estimate for the 1 s. d. statistical error $\delta\mathcal{S}_1 \simeq (\sqrt{2} \times 0.36) / \sqrt{N_{event}} \simeq 0.5 / \sqrt{N_{event}}$, where N_{event} is the number of events of type (12). In order to push $\delta\mathcal{S}_1$ below the percent level $N_{event} > 10^4$ events are needed – an unrealistic number even for the upgraded Tevatron. In the case of pp collisions at the LHC energy $\sqrt{s} = 14$ TeV, we have $\Delta\mathcal{O}_2 \approx \Delta\bar{\mathcal{O}}_2 \simeq 0.25$, which implies $|\mathcal{S}_2 / (\sqrt{2}\Delta\mathcal{O}_2)| \simeq 10^{-3}$. Although the production of 10^7 $t\bar{t}$ pairs may be expected at the Large Hadron Collider operating at high luminosity, the systematic errors of a measurement of our correlations at a hadron collider will probably be too large to probe effects of the order of a per mill.

One may ask whether there are better observables to trace transverse polarization than the ones we chose. Obvious variations are, for example, $\hat{\mathbf{p}}_p \cdot (\mathbf{k}_{\bar{t}} \times \mathbf{q}_{\ell^+})/s$ or $\hat{\mathbf{p}}_p \cdot (\hat{\mathbf{k}}_{\bar{t}} \times \mathbf{q}_{\ell^+})/\sqrt{s}$. Another variation would be $\hat{\mathbf{p}}_p \cdot (\mathbf{k}_{\bar{t}} \times \mathbf{q}_{\ell^+}) / |\mathbf{k}_{\bar{t}} \times \mathbf{q}_{\ell^+}|$. All of these observables lead to similar or smaller ratios $\mathcal{O}/\Delta\mathcal{O}$. We did not attempt to construct

fully optimized observables [13] here. A more thorough analysis would construct such observables, which maximize the signal-to-noise ratio, not only for the semileptonic $t\bar{t}$ decay channels discussed in this paper, but also for all other decay modes [25].

In conclusion we have computed the QCD-induced transverse polarization of t and \bar{t} quarks produced in high energetic $p\bar{p}$ and pp collisions. Resulting angular correlations which involve the t or \bar{t} decay products are at the percent level at Tevatron energies and at the per mill level at the LHC. As these are definite QCD predictions it will still be worthwhile to measure the correlations (15), (18), since they can be used as “sensors” for new physics effects in the top system: any observable effect — i.e., any significant deviation from the above results — would point towards strong $t\bar{t}$ final state interactions beyond the Standard Model forces.

Acknowledgements

A. B. would like to thank L. Dixon and Y. Shadmi for useful discussions.

References

- [1] F. Abe et al., CDF Collaboration, Phys. Rev. Lett. **74** (1995) 2626; S. Abachi et al., D0 Collaboration, Phys. Rev. Lett. **74** (1995) 2632.
- [2] G. L. Kane, J. Pumplin, and W. Repko, Phys. Rev. Lett. **41** (1978) 1689.
- [3] J. H. Kühn, A. Reiter, and P. Zerwas, Nucl. Phys. **B 272** (1986) 560.
- [4] M. Anselmino, P. Kroll, and B. Pire, Phys. Lett. **B 167** (1986) 113.
- [5] I. Bigi et al., Phys. Lett. **B 181** (1986) 157.
- [6] W. G. D. Dharmaratna and G. R. Goldstein, Phys. Rev. **D 41** (1990) 1731.
- [7] W. G. D. Dharmaratna and G. R. Goldstein, preprint TUFTS-TH-92-G02 (1992), unpublished.
- [8] A. Czarnecki, M. Jezabek, and J. H. Kühn, Nucl. Phys. **B 351** (1991) 70.
- [9] R. H. Dalitz and G. R. Goldstein, Phys. Rev. **D 45** (1992) 1531.
- [10] G. L. Kane, G. A. Ladinsky, and C.-P. Yuan, Phys. Rev. **D 45** (1992) 124.
- [11] W. Bernreuther, O. Nachtmann, P. Overmann, and T. Schröder, Nucl. Phys. **B 388** (1992) 53; **B 406** (1993) 516 (E); A. Brandenburg and J. P. Ma, Phys. Lett. **B 298** (1993) 211.
- [12] W. Bernreuther, J. P. Ma, and T. Schröder, Phys. Lett. **B 297** (1992) 318.
- [13] D. Atwood and A. Soni, Phys. Rev. **D 45** (1992) 2405.
- [14] T. Arens and L. M. Seghal, Nucl. Phys. **B 393** (1993) 46.
- [15] W. Bernreuther and A. Brandenburg, Phys. Lett. **B 314** (1993) 104; Phys. Rev. **D 49** (1994) 4481.
- [16] W. Bernreuther, J. P. Ma, and B. H. J. McKellar, Phys. Rev. **D 51** (1995) 2475.

- [17] J. G. Körner, A. Pilaftsis, and M. M. Tung, *Z. Phys.* **C 63** (1994) 575; S. Groote, J. G. Körner, and M. M. Tung, Mainz preprint MZ-TH/95-09 (1995).
- [18] R. Harlander, M. Jezabek, J. H. Kühn, and T. Teubner, *Phys. Lett.* **B 346** (1995) 137.
- [19] P. Haberl, O. Nachtmann, and A. Wilch, Heidelberg preprint HD-THEP-95-25 (1995).
- [20] M. Glück, J. F. Owens, and E. Reya, *Phys. Rev.* **D 17** (1978) 2324; B. L. Combridge, *Nucl. Phys.* **B 151** (1979) 429.
- [21] L. F. Abbott, *Nucl. Phys.* **B 185** (1981) 189; L. F. Abbott, M. T. Grisaru, and R. K. Schaefer, *Nucl. Phys.* **B 229** (1983) 372.
- [22] Z. Bern, L. Dixon, and D. A. Kosower, *Phys. Lett.* **B 302** (1993) 299; erratum *ibid.* **B 318** (1993) 649; *Nucl. Phys.* **B 412** (1994) 751.
- [23] K. Melnikov and O. Yakovlev, *Phys. Lett.* **B 324** (1994) 2171; V. S. Fadin, V. A. Khoze, and A. D. Martin, *Phys. Rev.* **D 49** (1994) 2247.
- [24] M. Glück, E. Reya, and A. Vogt, *Z. Phys.* **C 67** (1995) 433.
- [25] A. Brandenburg and P. Uwer, work in preparation.

Figure Captions

Fig. 1 One-loop Feynman diagrams for the process $q\bar{q} \rightarrow t\bar{t}$ which give a nonzero contribution to the function b_3^q defined in Eq. (3) through interference with the Born diagram.

Fig. 2 One-loop Feynman diagrams for the process $gg \rightarrow t\bar{t}$ which give a nonzero contribution to the function b_3^g through interference with the Born diagrams.

Fig. 3 Transverse polarization P_\perp^q (defined in Eq. (5)) as a function of the partonic c.m. energy $\sqrt{\hat{s}}$ and the cosine of the scattering angle z .

Fig. 4 Transverse polarization P_\perp^g (defined in Eq. (5)) as a function of the partonic c.m. energy $\sqrt{\hat{s}}$ and the cosine of the scattering angle z .

Fig. 5 Correlation \mathcal{S}_1 (defined in Eq. (15)) for proton-antiproton scattering as a function of the collider c.m. energy \sqrt{s} .

Fig. 6 Rapidity distribution $\langle \mathcal{O}_1 \delta(r_{\bar{t}} - r'_{\bar{t}}) \rangle_{\bar{t}\bar{t}^+}$ for $p\bar{p}$ collisions at $\sqrt{s} = 1.8$ TeV.

Fig. 7 Correlations \mathcal{S}_2 (full line) and Δ_2 (dashed line) (defined in Eqs. (18) and (19), respectively) for proton-proton collisions as a function of the collider c.m. energy \sqrt{s} .

Fig. 8 Rapidity distributions $\langle \mathcal{O}_1 \delta(r_{\bar{t}} - r'_{\bar{t}}) \rangle_{\bar{t}\bar{t}^+}$ (full line) and $\langle \bar{\mathcal{O}}_1 \delta(r_t - r'_t) \rangle_{t\bar{t}^-}$ (dashed line) for pp collisions at $\sqrt{s} = 14$ TeV.

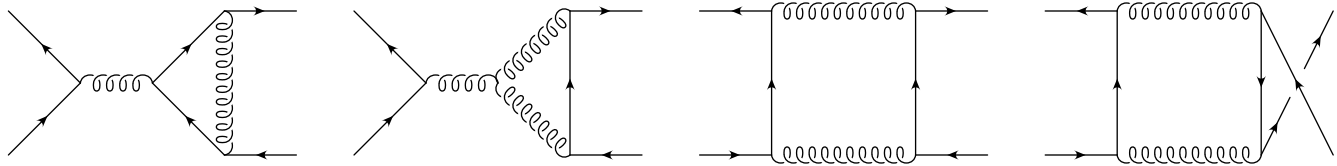


Fig. 1

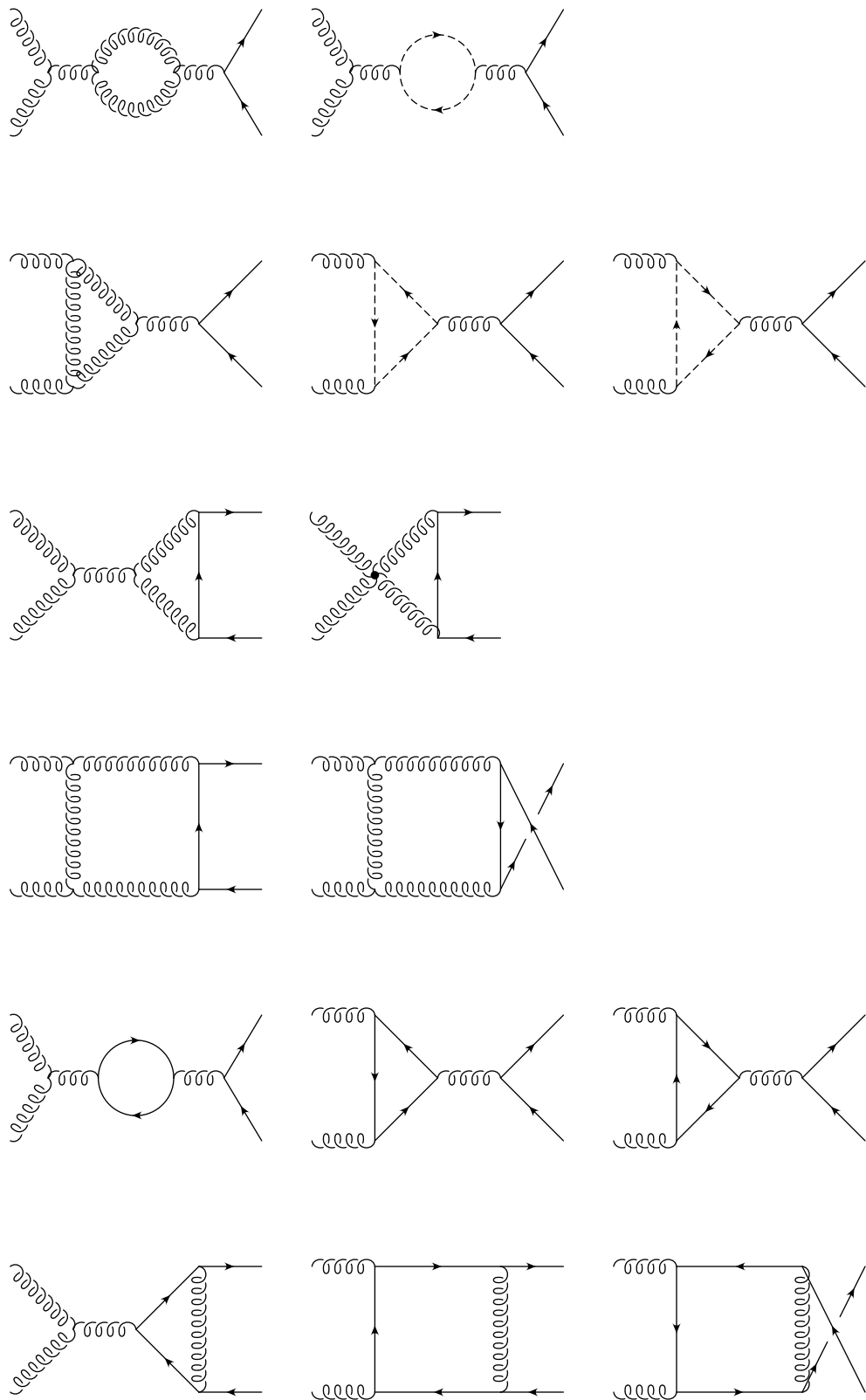


Fig. 2

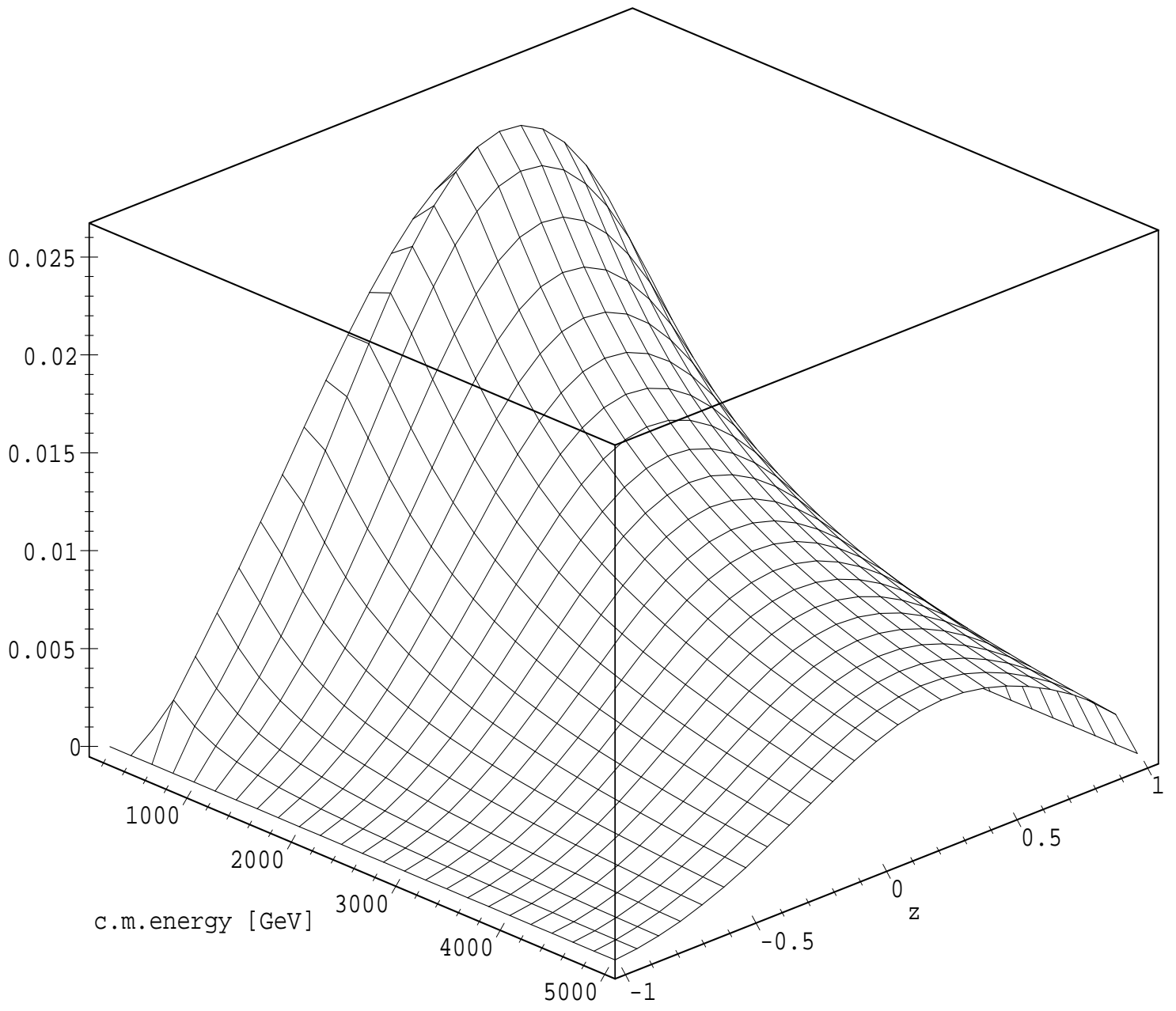


Fig. 3

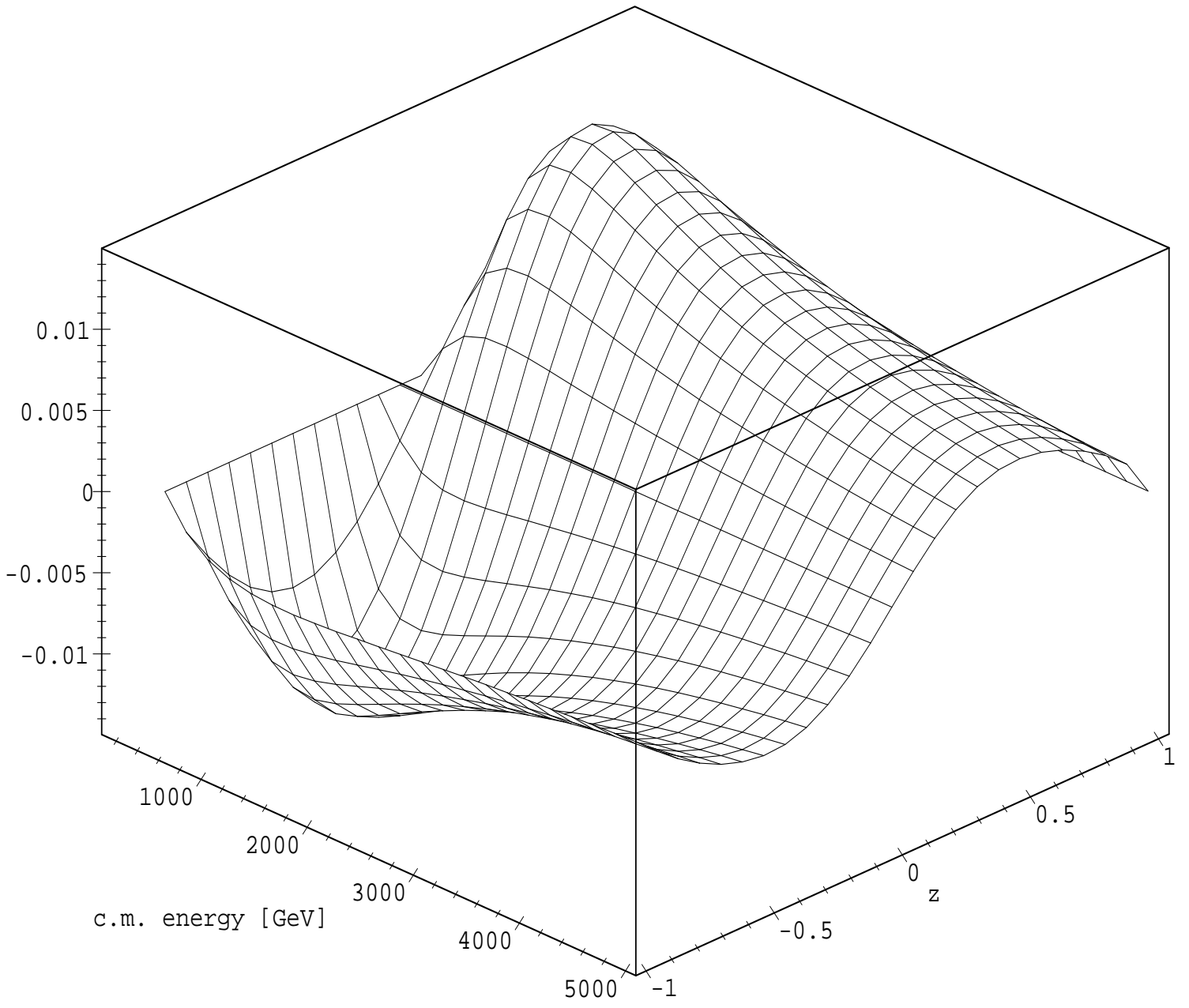
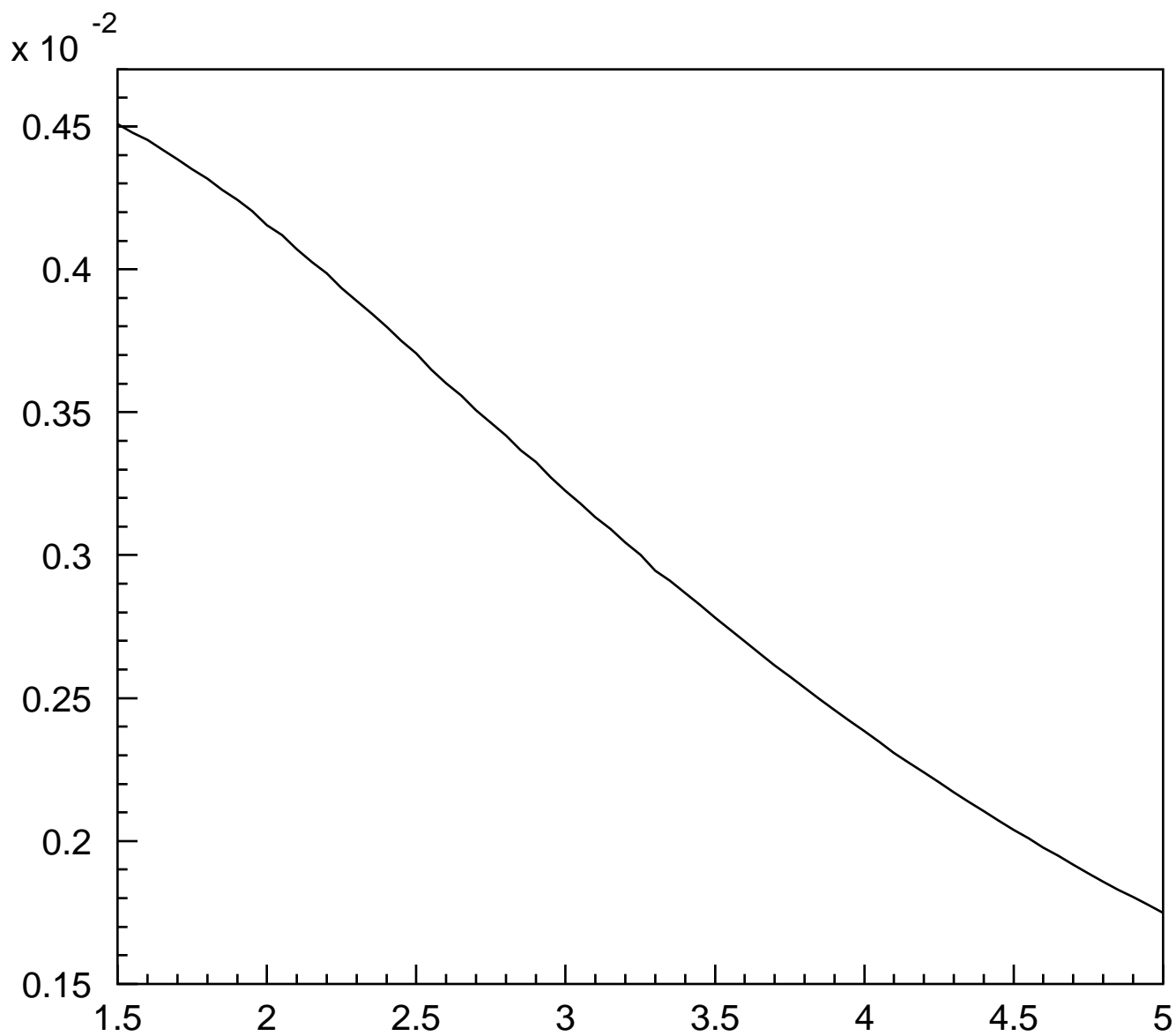


Fig. 4



\sqrt{s} [TeV]

Fig. 5

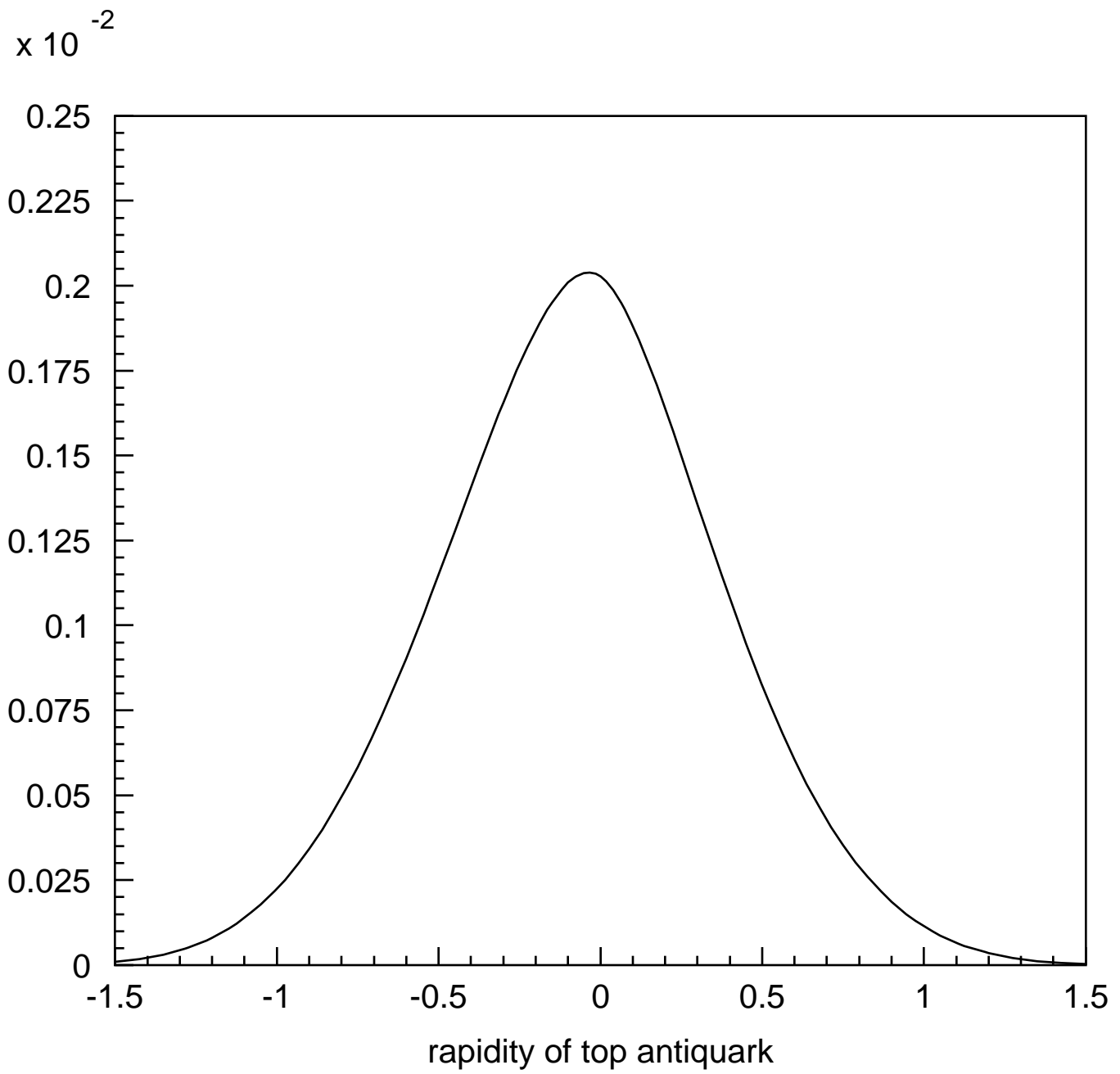


Fig. 6

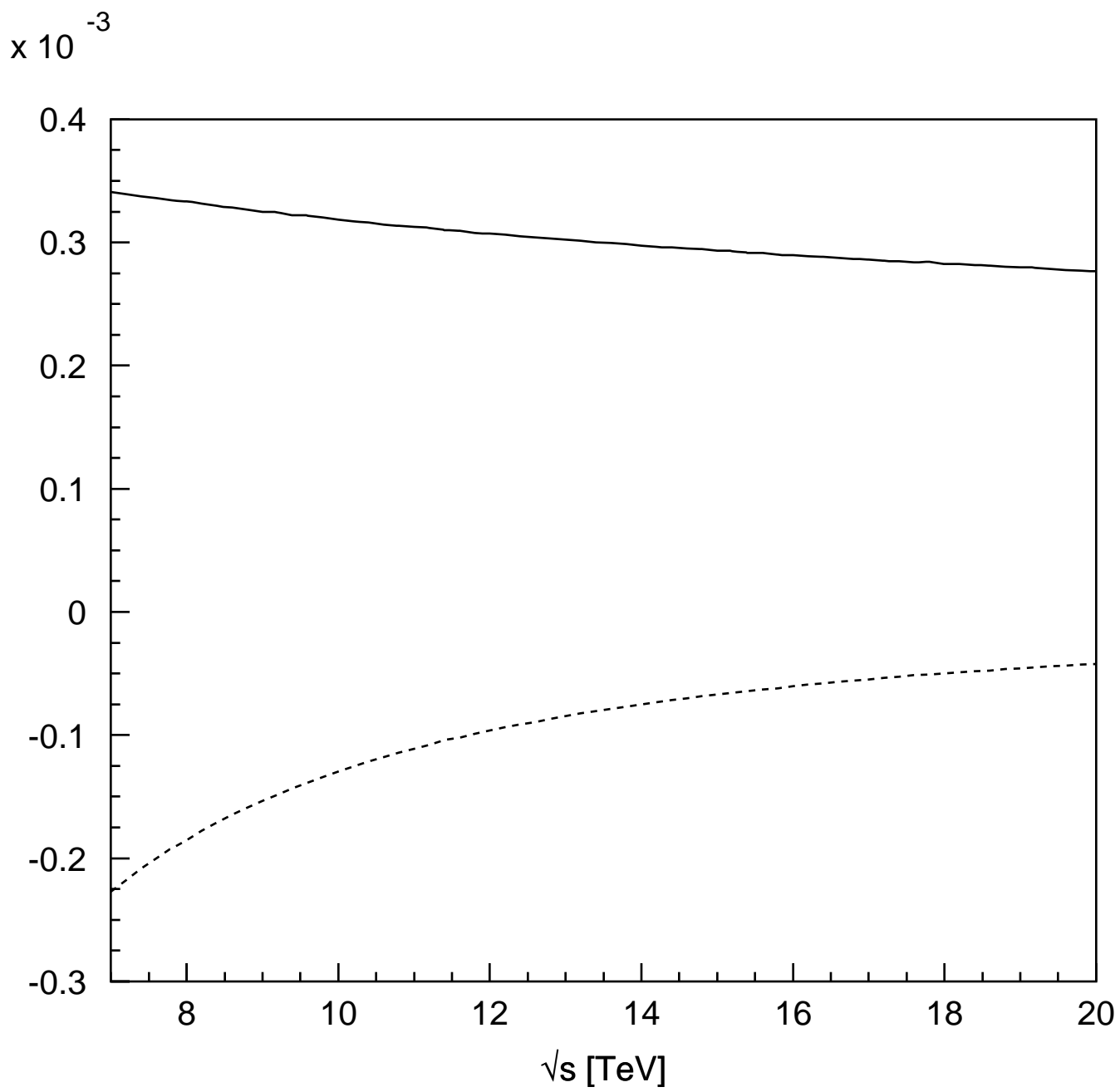


Fig. 7

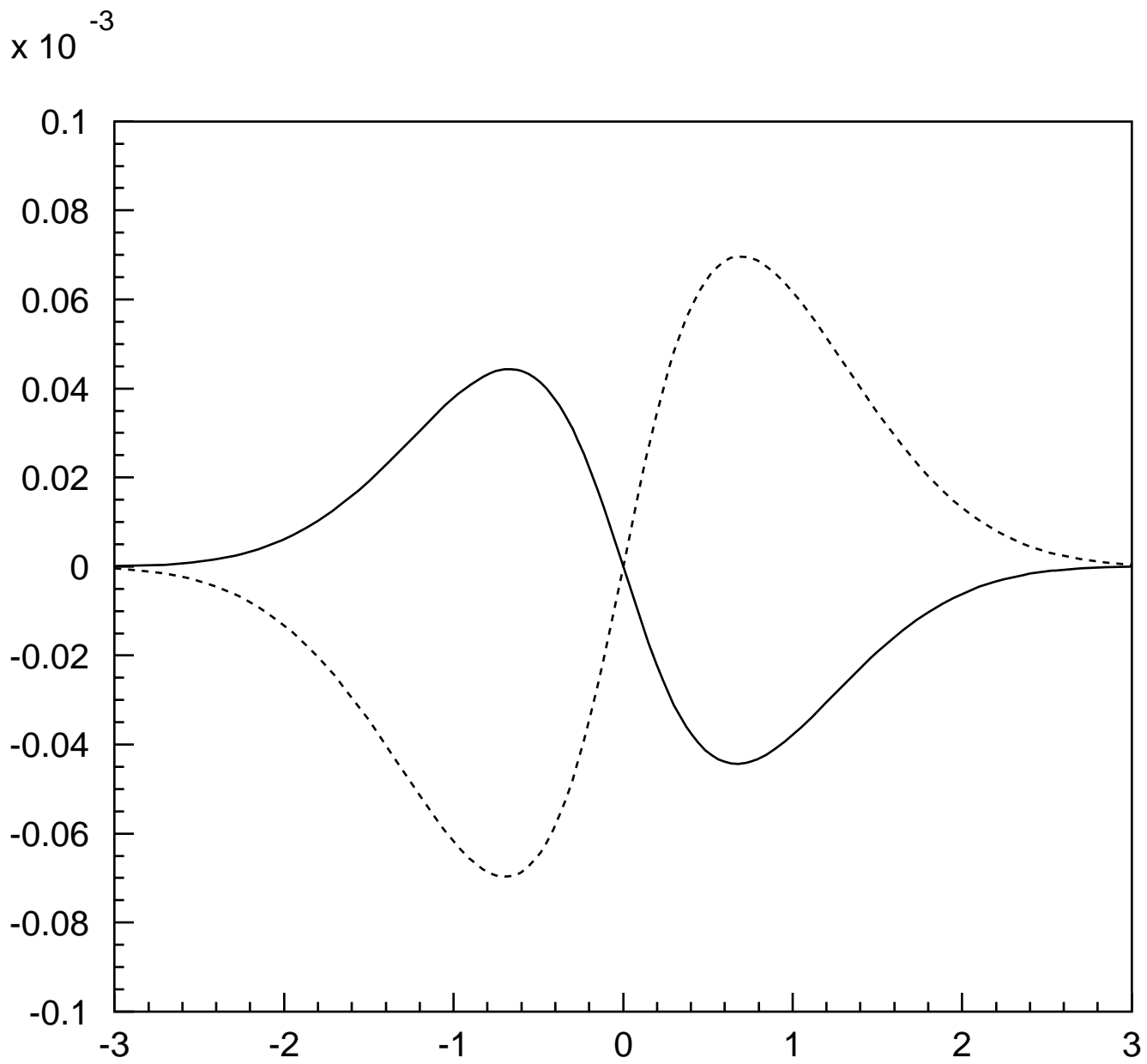


Fig. 8